Biophysical Journal, Volume *122*

Supplemental information

Remodeling of yeast vacuole membrane lipidomes from the log (one phase) to stationary stage (two phases)

John Reinhard, Chantelle L. Leveille, Caitlin E. Cornell, Alexey J. Merz, Christian Klose, Robert Ernst, and Sarah L. Keller

Supporting Material

Remodeling of vacuole membrane lipidome from the log stage (1-phase) to stationary stage (2-phases)

John Reinhard,[1,2,6] Chantelle L. Leveille,[3,6] Caitlin E. Cornell,[3] Alexey J. Merz,[4] Christian Klose,[5] Robert Ernst,[1,2]* Sarah L. Keller[3]*

1 Medical Biochemistry and Molecular Biology, Medical Faculty, Saarland University, Homburg, Germany
2 PZMS, Center for Molecular Signaling, Medical Faculty, Saarland University, Homburg, Germany
3 Department of Chemistry, University of Washington, Seattle, WA, USA
4 Department of Biochemistry, University of Washington, Seattle, WA, USA
5 Lipotype GmbH, Am Tatzberg 47, Dresden, Germany
6 These authors contributed equally to this work

**Correspondence: slkeller@uw.edu, robert.ernst@uks.eu*

This PDF file includes

Caption for Data File S1

Raw data for abundances of all lipids in vacuoles immuno-isolated with a Mam3 bait protein from yeast in the log stage (light gray), stationary stage (dark gray) and whole cell data from stationary cells (blue). Additional data of log stage whole cell lipidomes (Fig. S7, Logarithmic) and log stage lipidomes of vacuole membranes immuno-isolated via a Vph1 bait protein (Fig. S8, Vph1-bait) are taken from (1) and highlighted in green. Data in Figure S8 (Mam3-bait) are replotted from Figure S6 (Logarithmic). Tabs in the data file show calculated and plotted values for respective figures.

Supplemental Methods

Microscopy

Saccharomyces cerevisiae BY4741 (2, 3) expressing a Mam3-GFP fusion protein from its endogenous locus and promoter was used for fluorescence microscopy experiments. Live yeast cells were immobilized on a coverslip coated with 3 µL of 1 mg/mL concanavalin-A (EPC Elastin Products Co. catalog no. C2131) in buffer (50 mM HEPES at pH 7.5, 20 mM calcium acetate, and 1 mM $MnSO_4$). Immediately prior to use, the coverslips were washed with MilliQ water and dried with compressed air. Cells were diluted for imaging in an isosmotic solution of conditioned medium from the yeast culture. To produce conditioned medium, 1 mL of culture was centrifuged at 3,400 × g. The supernatant was collected and centrifuged again at 3,400 × g to remove all remaining cells. To decrease refractive index mismatch (4), 200 µL of OptiPrep (60% OptiPrep Density Gradient Medium; Sigma catalog no. D1556) was added to 800 µL of medium and vortexed. Samples of 3 µL of cells were diluted into 3 µL of conditioned medium containing 12% OptiPrep and placed onto the concanavalin-A–coated coverslip. A second coverslip was added to the top. Cells were allowed to adhere to the coated coverslip for 10 min before imaging. Unless otherwise noted, images were acquired on a Nikon TE2000 microscope equipped with a Teledyne Photometrics Prime 95BSI camera. Using an oil-immersion objective (100×, 1.4 numerical aperture), GFP was excited with an X-Cite 110 light-emitting diode light source and filtered through an infrared cut filter to prevent aberrant heating of the sample from the optics. Brightness and contrast were adjusted linearly using ImageJ software (https://imagej.nih.gov/ij/).

Preparation of magnetic beads

Dynabeads with Protein G (Thermo Fisher Scientific #10009D) from 1.6 mL of slurry were washed with 1.6 mL phosphate buffered saline containing 0.02 % Tween-20 (PBS-T). After resuspension in 1.6 mL fresh PBS-T, 10 µL of anti-FLAG antibody (M2, monoclonal mouse IgG1, affinity isolated, F1804, 1 mg/ml) was added to the Dynabeads to yield a sub-saturating coverage of the beads with antibody. The resulting mix was incubated overnight at 4°C with an overhead rotation at 20 rpm. The supernatant was removed and the antibody-coated magnetic beads were washed once with 1.6 mL of PBS-T and twice with 1.6 mL IP buffer (25 mM HEPES pH 7.0, 1 mM EDTA, 150 mM NaCl). Immediately before use in immuno-isolation, the supernatant was again discarded and replaced with 700 µL of fresh IP buffer.

Lipid extraction, lipidomics data acquisition and post-processing

Mass spectrometry-based shotgun lipidomics was performed by Lipotype GmbH (Dresden, Germany) as described (5, 6). Lipids were extracted using a two-step chloroform/methanol procedure (5). Samples were spiked with internal lipid standards for major lipid classes in which the lipids contain combinations of acyl chains not found in biological samples, as previously described (1). After extraction, the organic phase was transferred to an infusion plate and dried in a speed vacuum concentrator. 1st step dry extract was re-suspended in 7.5 mM ammonium acetate in chloroform/methanol/propanol (1:2:4, V:V:V) and 2nd step dry extract in 33 % ethanol solution of methylamine in chloroform/methanol (0.003:5:1; V:V:V). All liquid handling steps were performed using Hamilton Robotics STARlet robotic platform with the Anti Droplet Control feature for organic solvents pipetting.

Samples were analyzed by direct infusion on a QExactive mass spectrometer (Thermo Scientific) equipped with a TriVersa NanoMate ion source (Advion Biosciences). Samples were analyzed in both positive and negative ion modes with a resolution of Rm/z=200=280000 for MS and Rm/z=200=17500 for MSMS experiments, in a single acquisition. MS/MS was triggered by an inclusion list encompassing corresponding MS mass ranges scanned in 1 Da increments (7). Both MS and MSMS data were combined to monitor ergosterol-esters (EE), diacylglycerol (DAG) and triacylglycerol (TAG) ions as ammonium adducts; Phosphatidylcholine (PC) as an acetate adduct; and cardiolipin (CL), phosphatidic acid (PA), phosphatidylethanolamine (PE), phosphatidylglycerol (PG), phosphatidylinositol (PI) and phosphatidylserine (PS) as deprotonated anions. MS only was used to monitor the lyso-lipids of PA, PE, PI, and PS, as well as inositolphosphorylceramide (IPC), mannosyl-inositolphosphorylceramide (MIPC), and mannosyl-di-(inositolphosphoryl)ceramide (M(IP)2C) as deprotonated anions; ceramine (Cer) and lyso-PC

(LPC) as acetate adducts and ergosterol as protonated ion of an acetylated derivative (8). One source of error that can arise is when fatty acids form an adduct with other molecules in the sample. This type of error is more likely when longer, multi-step procedures are used to isolate membrane lipids, as in immuno-isolation as opposed to a fast extraction of all lipids from the entire cell.

Data were analyzed with in-house developed lipid identification software based on LipidXplorer (9, 10). Data post-processing and normalization were performed using an in-house developed data management system. Only lipid identifications with a signal-to-noise ratio >5, and a signal intensity 5-fold higher than in corresponding blank samples were considered for further data analysis.

Microsomal preparation

Throughout microsomal preparation and immuno-isolation procedures (Fig. 2 of the main text), samples from the supernatant and pellet fractions were retained for a subsequent immunoblot analysis. Break points are indicated where samples can be stored at -80°C. 4,000 OD_{600}·mL of yeast cells were required as starting material for isolating vacuole membranes from log stage cells. For stationary stage cells, whose mechanical disruption is less efficient (Fig. S1E), 17,200 OD_{600}·mL were used. Cells were harvested from the culture by centrifugation at 3,000 x g for 5 min at room temperature. The resulting pellet was resuspended in 25 mL of pre-chilled phosphate buffered saline (PBS) and placed on ice. Cell suspensions corresponding to 1,000 OD_{600}·mL (8,600 OD_{600}·mL for stationary stage) were transferred to 50 ml tubes and centrifuged at 3,000 x g for 5 min at 4°C. After discarding the supernatants, the cell pellets were snap frozen in liquid nitrogen and stored at -80°C until further use.

A cell pellet corresponding to 1,000 OD_{600}·mL (2,150 OD_{600}·mL for stationary stage) was thawed on ice and then resuspended in 10 mL of microsome preparation (MP) buffer (25 mM HEPES at pH 7.0, 1 mM EDTA, 0.6 M mannitol, to which 30 µg/ml protease inhibitor cocktail (10 µg/mL of pepstatin, antipain, chymotrypsin each) and 12.5 units/mL benzonase was added freshly). To mechanically lyse the cells (Fig. 2A), 13 g pre-chilled zirconia glass beads (0.5 mm diameter) were combined with cell suspension in a 15 mL tube. Additional MP buffer was added to the suspension to fill the reaction tube and to avoid the formation of air bubbles during mechanical agitation. Using a FastPrep-24 bead beater at 4°C, cells were subjected to 10 cycles of shaking for 15 s at 5 m/s, followed by 45 s of cooling on ice. The resulting cell lysates were transferred to fresh 15 mL tubes. 2 mL MP buffer were used to wash the zirconia glass beads and then combined with the previous lysates.

Differential centrifugation was performed to separate a crude microsomal membrane fraction from both cell debris and soluble proteins, thereby enriching cellular membranes including vacuole membranes (Fig. 2A). Cell lysates were spun at 3,234 x g and 4°C for 5 min in a swinging bucket rotor. The supernatant was transferred to a fresh 15 ml tube and re-centrifuged at 3,234 x g and 4°C for 5 min. The resulting supernatant (S3) was then transferred to ultracentrifuge bottles (26.3 mL polycarbonate bottle assemblies, Beckman Coulter #355618), balanced with MP buffer and centrifuged (rotor Type 70 Ti) at 12,000 x g and 4°C for 20 min. The resulting supernatant (S12) was transferred to a fresh ultracentrifuge bottle, balanced with MP buffer, and centrifuged at 100,000 x g at 4°C for 60 min. Although vacuole markers Vph1 and Vac8 are also found in the pellet after 12,000 x g centrifugation (P12) and in the supernatant after 100,000 x g centrifugation (S100), we chose to work with the pellet after 100,000 x g centrifugation (P100) because it contains smaller vesicles that are less likely connected to mitochondria and lipid droplets. To avoid contamination of the microsome pellet (P100) by lipid droplets floating on top of the supernatant (S100), the supernatant was removed by vacuum from the ultracentrifuge tube, working carefully from the top to the bottom. The pellet containing crude microsomes (P100) was rinsed with 15 mL of MP buffer to remove remnants of the supernatant before resuspending it in 1 mL MP buffer, snap freezing the sample in liquid nitrogen, and storage at -80°C until further use.

Pellets from the microsomal preparation were thawed from -80°C slowly on ice and then sonicated to segregate aggregated membrane vesicles and to break vacuoles into smaller vesicles (Fig. 2A of the main text) (1). A tip sonicator (MS72 sonotrode on a Bandelin Sonopuls HD 2070) was used for 10 s, with a duty cycle of 0.7 at 50% amplitude, keeping the samples on ice. Previous experiments revealed that this treatment does not cause membrane mixing (1). Notably, sonication cleared the originally cloudy suspension. After centrifugation at 3,000 x g at 4°C for 3 min, the supernatant containing microsomes was used for subsequent immuno-isolations procedures.

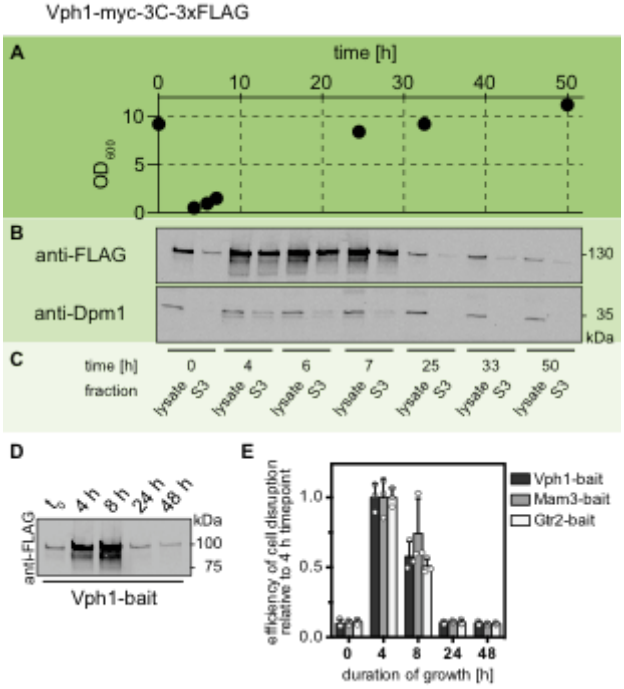

Figure S1: The level of the Vph1-bait protein (Vph1-myc-3C-3xFLAG) is low in the stationary stage compared to the log stage. (A) Yeast growth curve through time, where OD_{600} is the optical density at 600 nm, a proxy for the density of cells. The sample at time "0" is a preculture after 19 hours of the preculture's growth. The preculture was then diluted to OD_{600} = 0.1 and allowed to grow into the log (early time points), and stationary stage (late time points). **(B-C)** At each timepoint, an immunoblot was performed for the cell lysate (left columns) and supernatant ("S3", right columns). The supernatant corresponds to S3 in Fig. 2, which is collected from the supernatant after the first step of microsome preparation, a 3,234 x g centrifugation. The presence of Vph1-bait was visualized by anti-FLAG primary and fluorescent secondary antibodies. In the log stage, Vph1 is abundant (timepoints 1-3) in the cell lysate and S3 samples. This result is consistent with reported values of > 50,000 copies/cell, which likely applies only to the log stage (up to ~10 hours of growth) (11, 12). In the stationary stage (timepoints 4-6), Vph1 is significantly reduced in the cell lysate and further reduced after centrifugation step S3. Dpm1, a protein that is a marker for the endoplasmic reticulum, is used as a control. Dpm1 is reported to have < 2,000 copies/cell (11). It maintains a roughly constant abundance throughout the growth cycle. **(D)** A minimal experiment reproducing the results in panel B, with time points similar to Fig. 3C. **(E)** The efficiency of mechanical cell disruption differs with the growth stage. Cell disruption efficiency was estimated by measuring the protein concentration in the post-nuclear supernatant (after a 3,234 x g centrifugation) of cell lysates. The measured protein concentrations are normalized to the concentration measured for cells cultivated for 4 h prior to cell harvest and cell lysis. Experiments were performed in biological triplicates for yeast strains containing one of three distinct immuno-isolation baits (Vph1-bait, Mam3-bait, Gtr2-bait).

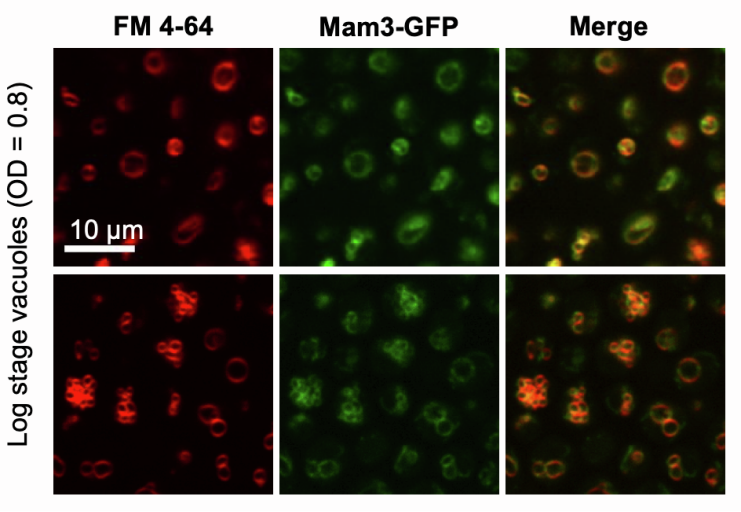

Figure S2: Mam3-GFP localizes to the vacuole membrane. The protein Mam3-GFP (middle column) colocalizes with FM 4-64 (left column), which is known to label vacuole membranes. All yeast in the field of view are living and in the logarithmic stage; no micron-scale domains appear in their membranes. Images were taken at room temperature.

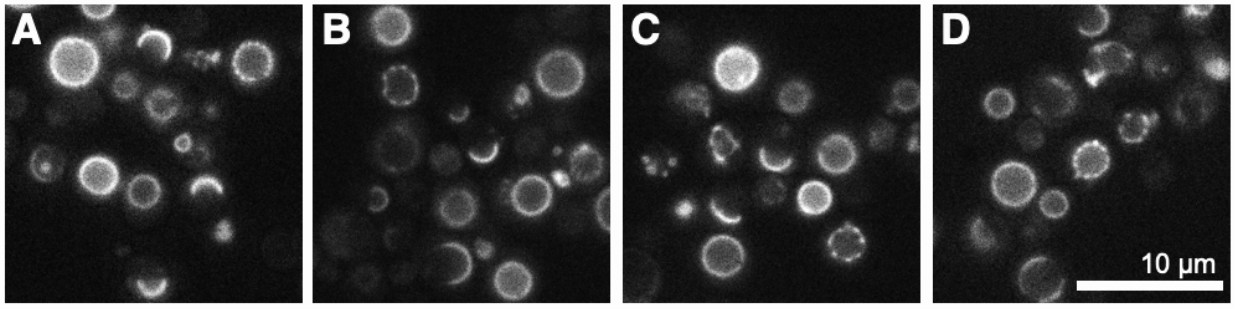

Figure S3: Stationary stage vacuoles phase separate as shown via Mam3-GFP. (A-D) Four fields of view of vacuole membranes in living yeast cells in the stationary stage after 48 hours of cultivation, under conditions equivalent to the cells in Figure S2. Bright areas of the membranes contain the fluorescent protein Mam3-GFP, which was endogenously labeled. Most vacuole membranes in the field of view have phase-separated into co-existing micron-scale domains. Images were taken at room temperature.

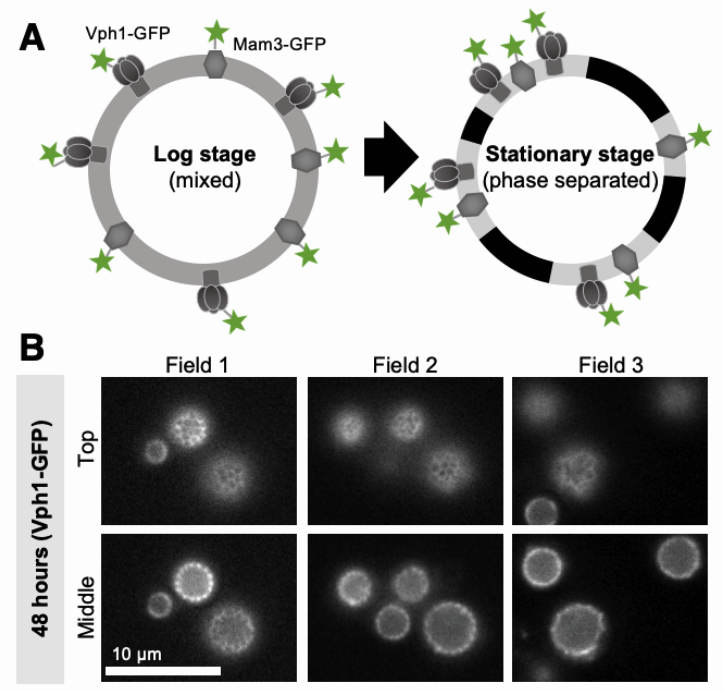

Figure S4: Stationary stage vacuoles phase separate as shown via Vph1-GFP. (A) Left: For yeast in the logarithmic stage, lipids and proteins appear uniformly distributed across the surface of vacuole membranes. Two of the proteins, Vph1 and Mam3, can be endogenously labeled with GFP (as shown here) or equipped with a C-terminal bait tag for subsequent immuno-isolations. **Right:** In the stationary stage, the vacuole membrane separates into two liquid phases. Vph1-GFP and Mam3-GFP preferentially partition to the same phase. **(B)** After 48 hours of growth, yeast are in the stationary stage and most vacuole membranes have phase separated. The proteins Mam3 (Fig. 3) and Vph1 partition into only one of the phases, shown at both the top and the midplane of the vacuoles in each field of view. Images are of living cells and were taken at room temperature.

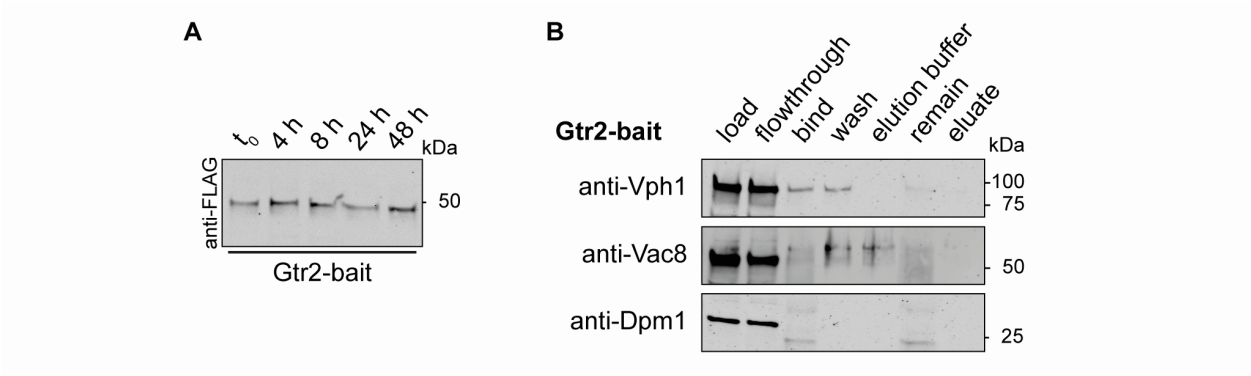

Figure S5: Immuno-isolation via the Gtr2-bait does not work. Gtr2 is a membrane-associated protein anchored to the vacuole membrane via a lipid anchor. In phase-separated, stationary stage vacuole membranes, it resides in the Lo phase (13). **(A)** The Gtr2-bait protein is equally abundant throughout the logarithmic and stationary growth stages. **(B)** We were not able to immuno-isolate any membranes via the Gtr2-bait protein using the MemPrep technology as described in Figure 2. In immunoblot analyses, the vacuole markers Vph1 and Vac8 are not detectable in the eluate. A corresponding figure for isolation via the Mam3-bait protein can be found in Figure 4.

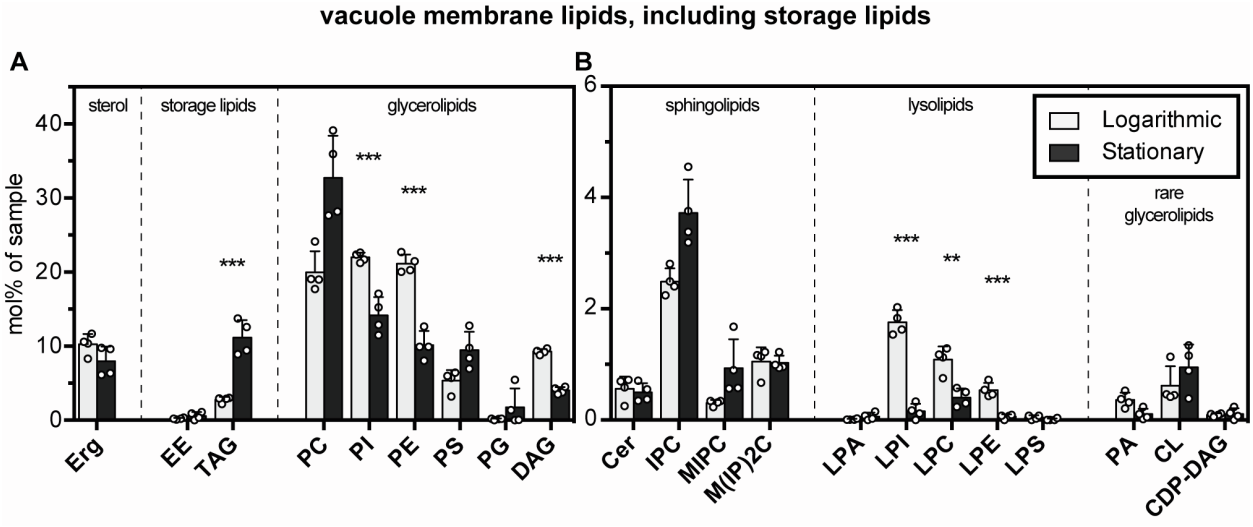

Figure S6: Lipids in log stage and stationary stage vacuole membranes immuno-isolated via a Mam3-bait protein, including storage lipids of ergosterol esters and TAG. Acronyms of lipid names are listed in Figure 5B. **(A)** Ergosterol, storage lipids and abundant glycerolipids. **(B)** Sphingolipids, lysolipids and rare glycerolipids. Note that the y-axis range covers a different range in panel (B) compared to panel (A) to highlight also low abundant lipids. Error bars are standard deviations of vacuole samples immuno-isolated on four different days. Data in this figure include the storage lipids of ergosterol esters and TAG, which are predominantly found in lipid droplets. For yeast in the log stage, we find that ergosterol esters constitute 0.3% of all isolated lipids, in contrast to 4.2% found by Zinser *et al*. (14). Specifically, Zinser *et al*. find a molar ratio of ergosterol to phospholipids of 0.18 and a molar ratio of ergosterol ester to ergosterol of 0.29 (14). Statistical significance was tested by multiple t-tests correcting for multiple comparisons (method of Benjamini *et al*. (15)), with a false discovery rate Q = 1%, without assuming consistent standard deviations. The symbols *, **, and *** denote $p < 0.05$, $p < 0.01$, and $p < 0.001$, respectively.

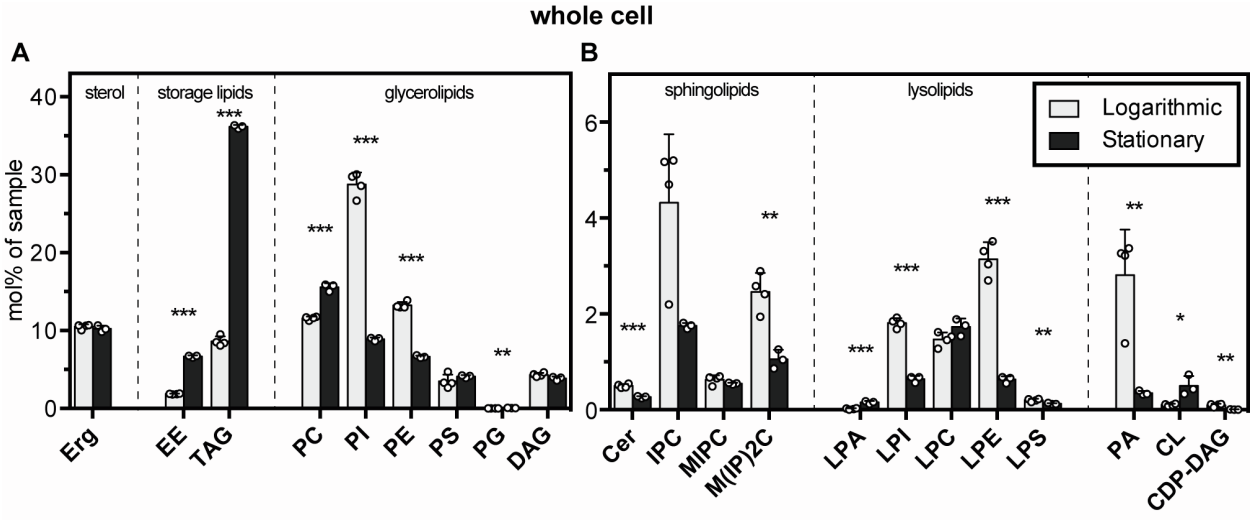

Figure S7: Whole cell lipidomes of cells in the log and the stationary stage. (A) Ergosterol, storage lipids and abundant glycerolipids. **(B)** Sphingolipids, lysolipids and rare glycerolipids. Error bars represent standard deviations of four independent experiments in the logarithmic stage and three independent experiments in the stationary stage. The data from logarithmic cells are taken from (1). Statistical significance was tested by multiple t-tests correcting for multiple comparisons (method of Benjamini *et al*. (15)), with a false discovery rate Q = 1%, without assuming consistent standard deviations. The symbols *, **, and *** denote $p < 0.05$, $p < 0.01$, and $p < 0.001$, respectively.

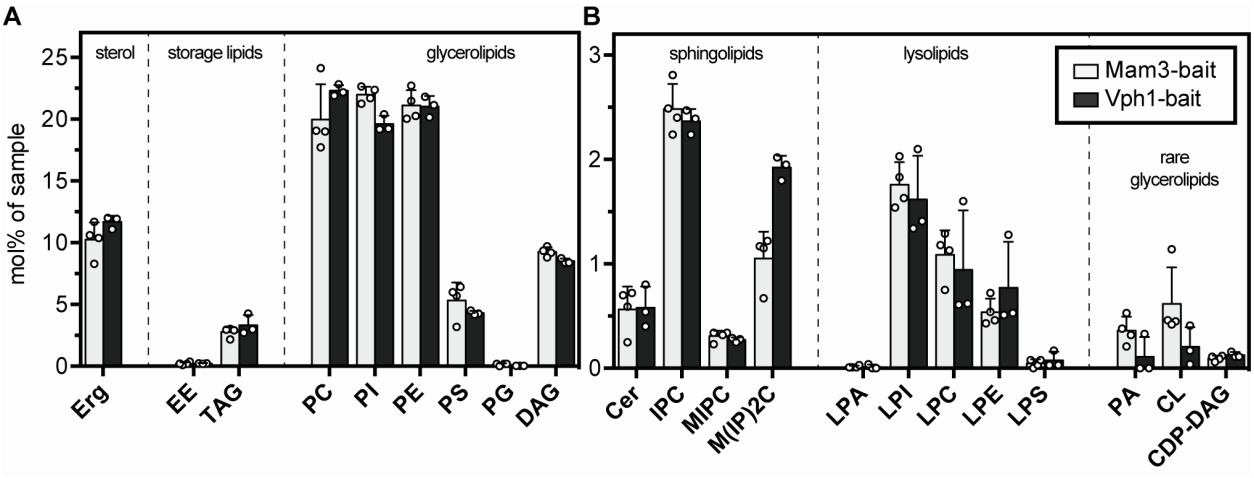

Figure S8: Comparison of lipidomes of vacuole membranes from yeast in the log stage isolated either with the Mam3-bait or the Vph1-bait. Data from membrane preparations via the Vph1-bait are replotted from Reinhard *et al*. (1). Mam3 data are replotted from Figure S6 (Logarithmic). Error bars represent the standard deviations of data from independent immuno-isolations performed on different days. Overall, the two lipidomes are in close agreement. The only apparent differences are in the amount of M(IP)2C (which may be inconsequential because it is in low abundance and which can change rapidly in its abundance during the log stage of growth (16)). These differences might reflect real disparities in how vacuole membranes are isolated by Vph1 and Mam3 baits, or they might reflect experimental variation. Full Vph1 data are presented and discussed in (1). **(A)** Three classes of lipids (glycerolipids, sterol and storage lipids) represent a majority of the lipidome. **(B)** Other classes of lipids (e.g. sphingolipids and ceramides) are much less abundant. Note that the y-axis range is roughly an order of magnitude smaller in panel B than in panel A. Statistical significance was tested by multiple t-tests correcting for multiple comparisons using the method of Benjamini *et al*. (15), with a false discovery rate Q = 1%, without assuming consistent standard deviations. All differences are non-significant.

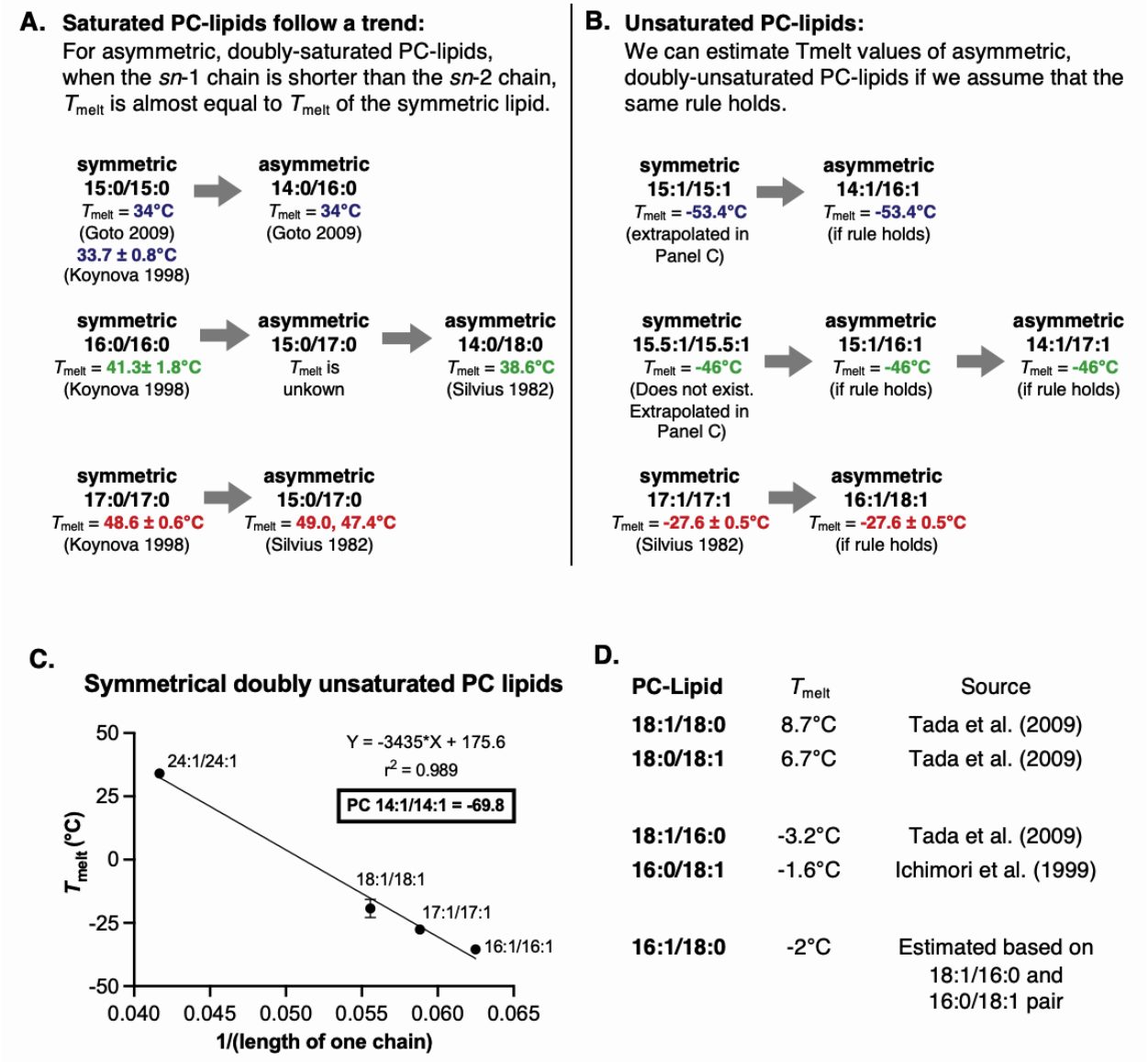

Figure S9: Experimental trends used to estimate melting temperatures for PC-lipids.

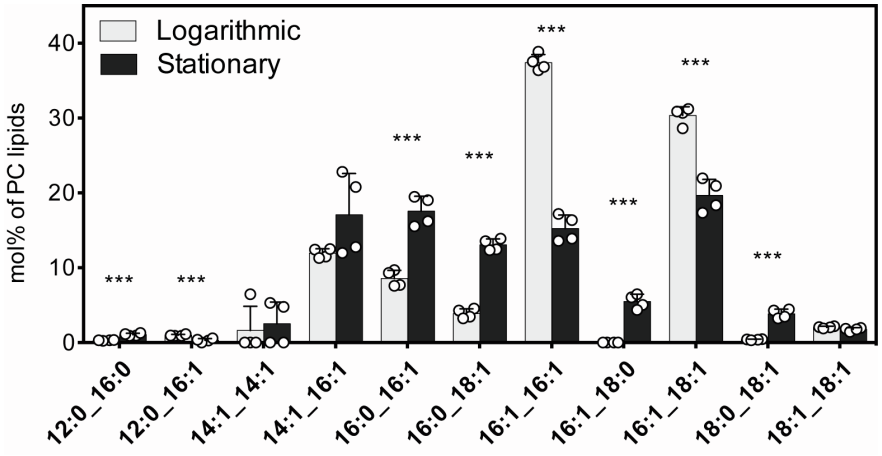

Figure S10: The species composition of vacuolar PC is distinct between log and stationary stage. The mole percent of PC lipids with different acyl chains in immuno-isolated vacuole membranes from yeast in the logarithmic and stationary stages are shown. Data are from four independent immuno-isolations with the error bars indicating the standard deviation. Data for lipids contributing less than 1 mol% in both the log and stationary stage are not shown. Statistical significance was tested by multiple t-tests correcting for multiple comparisons (method of Benjamini *et al*. (15)), with a false discovery rate Q = 1%, without assuming consistent standard deviations. The symbols *, **, and *** denote $p < 0.05$, $p < 0.01$, and $p < 0.001$, respectively.

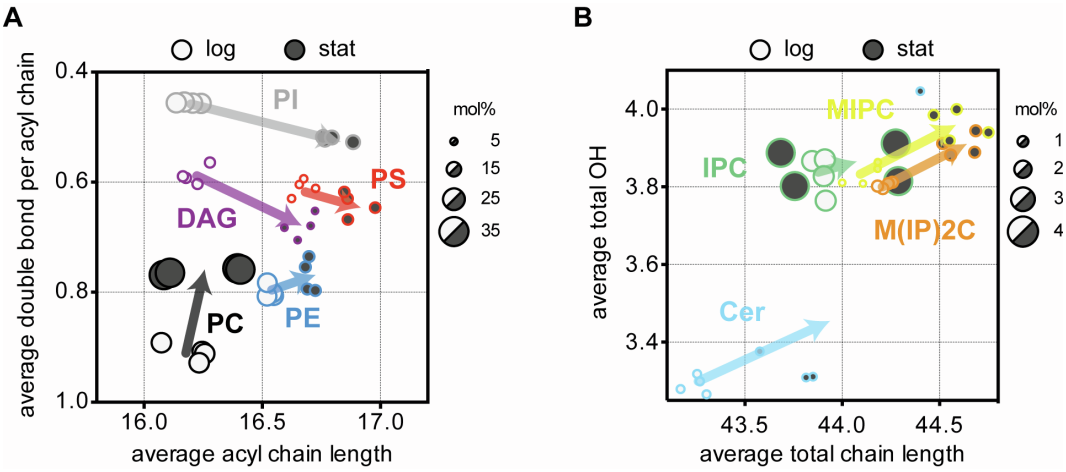

Figure S11: Remodeling of the lipid acyl chain composition in membrane lipids from log to stationary stage. (A) Average number of double bonds per acyl chain and average acyl chain length in the log (open circle) and stationary stage (filled circle) for several lipid types. The size of the circles corresponds to lipid abundance (in mol%) in immuno-isolated vacuole membranes for PC, PE, DAG, PS, and PI, excluding storage lipids such as triacylglycerols and ergosterol esters. Individual data points are derived from four independent immuno-isolations performed on different days. The arrows highlight changes in lipid saturation and the acyl chain length in the indicated lipid classes. **(B)** The same type of representation as in (A) for low abundance lipids of Cer, IPC, MIPC, and M(IP)$_2$C. Note that the y-axis in Panel B shows the average number OH groups in the lipid acyl chain region and that the x-axis shows the total chain length of the two lipid acyl chains of the respective sphingolipid.

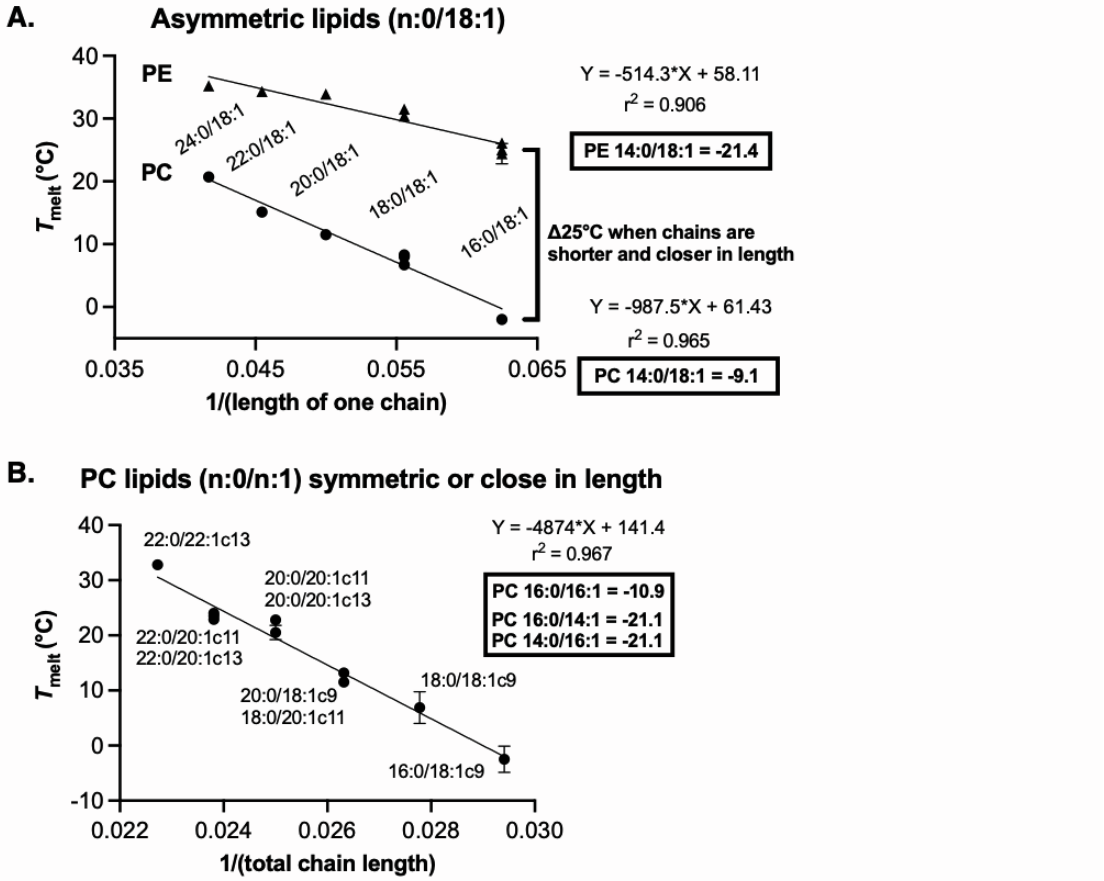

C.

Lipid	T_{melt}	Source
PE 16:1/16:1	-33.5°C	Koynova and Caffrey (1994)
PE 18:1/18:1	-16°C	Silvius (1982)
PE 16:1/18:1	-24.75°C	Estimated halfway in between 16:1/16:1 and 18:1/18:1
PC 16:0/16:1	-10.9°C	Extrapolated from F
PE 16:0/16:1	14.1°C	Estimated to be ~25°C higher than PC 16:0/16:1 based on difference in E where chains shorter and are closer in length
PE 16:0/18:1	25°C	Koynova and Caffrey (1994)
PE 14:0/18:1	21.4°C	Extrapolated from E
		(The difference between these is 3.6°C)
PE 16:0/16:1	14.1°C	Estimated above
PE 14:0/16:1	10.5°C	Estimated to be 3.6°C less

Figure S12: Trends used to estimate melting temperatures for PE-lipids.

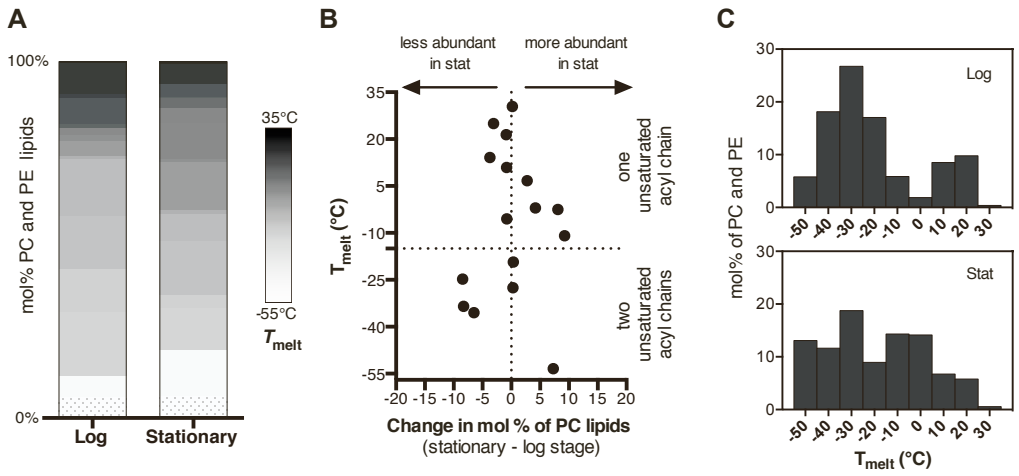

Figure S13: (A) Distributions of melting temperatures for PC and PE lipids of yeast vacuoles, in ratios corresponding to log and stationary stage vacuoles. In other words, the data are weighted to account for the increase in PC lipids and the decrease in PE lipids from the log stage to the stationary stage. **(B)** Changes in mol% of PC and PE lipids (x-axis) for each melting temperature (y-axis). The change in average lipid T_{melt} due to PC lipids is offset by a decrease in the fraction of PE lipids. **(C)** Histograms of the percent of PC and PE lipids at each melting temperature, in the log and stationary stages of growth. If we treat the data in the histograms as if they are independent points in a scatterplot, then the values would have standard deviations of 17°C in the log stage and 21°C in the stationary stage.

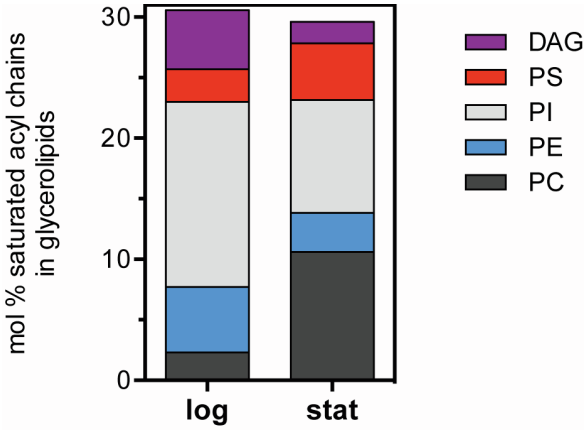

Figure S14: The total molar fraction of saturated fatty acyl chains in glycerolipids with two acyl chains is ~30 mol% in both the logarithmic and stationary stages. Data in the bar charts show that the distribution of saturated fatty acyl chains among different glycerolipid classes shifts from the logarithmic (log) to the stationary (stat) phase. For example, chains of PC lipids become much more saturated. Data are shown only for glycerophospholipid classes with an abundance of at least 0.5 mol%. Colors in the bar chart are in the same order, from top to bottom, as in the legend.

Table S1: Mole percent phospholipids in log-stage, isolated vacuole membranes
(Renormalized to sum all phospholipids to 100%)

Source	*PC*	*PE*	*PI*	*PS*	*PA*	*Lyso*	*CL*	*Other*	*Method*
Zinser 1991	*46.5*	*19.4*	*18.3*	*4.4*	*2.1*		*1.6*	*7.7*	*density gradient*
Tuller 1999	*39.2 ±3.3*	*26.6 ±1.5*	*24.4 ±1.8*	*3.9 ±1.0*	*2.5 ±0.8*	*1.6 ±0.8*	*0.4 ±0.1*	*1.4 ±0.1*	*density gradient*
Reinhard 2022	*31.4 ±1.0*	*29.6 ±1.5*	*27.6 ±0.6*	*6.1 ±0.3*	*0.2 ±0.3*	*4.7 ±1.9*	*0.3 ±0.3*	*0.2 ±0.0*	*immuno-isolation*
This work	*27.3 ±3.0*	*28.9 ±1.0*	*30.2 ±1.6*	*7.3 ±2.2*	*0.5 ±0.2*	*4.7 ±0.2*	*0.8 ±0.4*	*0.2 ±0.1*	*immuno-isolation*

Conditions for the experiments above:

	Strain	Glucose	Temp	Media	OD	Stage/Hours
Zinser 1991	*X-2180*	*3%*	*–*	*YPD*	*–*	*–*
Tuller 1999	*FY1679*	*2%*	*30˚C*	*YPD*	*?*	*Late log (~16 h)*
Reinhard 2022	*BY4741*	*2%*	*30˚C*	*SCD*	*1*	*Mid log (8 h)*
This work	*BY4741*	*2%*	*30˚C*	*SCD*	*1*	*Mid log (8 h)*

Notes: Uncertainties are standard deviations. Zinser *et al*. did not provide values of uncertainties (14). Tuller *et al*. note that FY1679 cells are atypical in their high fractions of palmitic acid (16:0) carbon chains and low fraction of oleic acid (18:1) chains (17), implying that comparisons between strains may not always be valid. A contamination of 0.4% cardiolipin in vacuoles isolated by Tuller *et al*. represents 5.5% contamination by mitochondrial membranes (of which 7.2 ± 0.2% of lipids are cardiolipin) (17). In the row titled “This work”, the entry for “Other” denotes PG lipids. If sphingolipids (IPC, MIPC, and MI(IP)2C) are included in “Other”, the mole percent of other lipids for this work increases to 5.0 ± 0.8%

Table S2: Values of T_{melt} for lipids in yeast vacuole membranes

PC Lipid:	T_{melt} (°C)	Source of T_{melt} value
14:1/14:1	-69.8	Extrapolated in Fig. S9, panel C
14:1/16:1	-53.4	Estimated in Fig. S9, panel B
16:0/16:1	-10.9	Estimated in Fig. S9, panel B
16:0/18:1	-2.5 ± 2.4	Koynova & Caffrey (1998), (18)
16:1/16:1	-35.5	Silvius (1982), (19)
16:1/18:0	-2	Estimated in Fig. S9, panel D
16:1/18:1	-27.5 ± 0.6	Silvius (1982), (19)
18:0/18:1	6.7	Tada (2009), (20)
18:1/18:1	-19.3 ± 3.6	Silvius (1982),(19)

PE Lipid:	T_{melt} (°C)	Source of T_{melt} value
14:0/16:1	10.5	Estimated in Fig. S12, panel C
14:0/18:1	21.4	Extrapolated in Fig. S12, panel A
16:0/16:1	14.1	Estimated in Fig. S12, panel C
16:0/18:1	25	Wang (1994), (21)
16:1/16:1	-33.5	Koynova & Caffrey (1994), (22)
16:1/18:1	19.5	Estimated in Fig. S12, panel C
18:0/18:1	30.4	Silvius (1982), (19)
18:1/18:1	-5.5 ± 0.5	Matsuki *et al*. (2017), (23)

When values of lipid melting temperatures are directly available in the literature, the reference is given. Values that are not directly available from the literature were extrapolated or estimated in Fig. S9 and S12.

Table S3: Literature values of T_{melt} for PC-lipids

(Used for estimating T_{melt} values for vacuole lipids)

Chain length : unsaturation	T_{melt} (˚C)	Reference	Reference #
13:0/13:0 PC	13.5	Silvius (1982)	(19)
14:0/14:0 PC	24	Goto *et al*. (2009)	(24)
15:0/15:0 PC	34 33.7 ± 0.8	Goto *et al*. (2009) Koynova & Caffrey (1998)	(18, 24)
16:0/16:0 PC	41.3 ± 1.8	Koynova & Caffrey (1998)	(18)
17:0/17:0 PC	48.6 ± 0.6	Koynova & Caffrey (1998)	(18)
14:0/16:0 PC	34	Goto *et al*. (2009)	(24)
14:0/18:0 PC	38.6	Silvius (1982)	(19)
15:0/17:0 PC	49.0, 47.4	Silvius (1982)	(19)
16:1/16:1 PC	-35.5, -36	Silvius (1982)	(19)
17:1/17:1 PC	-27.6 ± 0.5	Silvius (1982)	(19)
18:1/18:1 PC	-19.3 ± 3.6	Silvius (1982)	(19)
24:1c9/24:1c9 PC	34	Koynova & Caffrey (1998)	(18)
16:0/18:1 PC	-1.6	Ichimori *et al*. (1999)	(25)
18:1/16:0 PC	-3.2	Tada *et al*. (2009)	(20)
18:0/18:1 PC	6.7	Tada *et al*. (2009)	(20)
18:1/18:0 PC	8.7	Tada *et al*. (2009)	(20)
20:0/18:1 PC	11.5 ± 0.5	Koynova & Caffrey (1998)	(18)
22:0/18:1 PC	15.1	Koynova & Caffrey (1998)	(18)
18:0/20:1c11 PC	13.2	Koynova & Caffrey (1998)	(18)
20:0/20:1c11 PC	20.5 ± 1.3	Koynova & Caffrey (1998)	(18)
20:0/20:1c13 PC	22.8	Koynova & Caffrey (1998)	(18)
22:0/20:1c11 PC	22.9	Koynova & Caffrey (1998)	(18)
22:0/20:1c13 PC	23.5, 24	Koynova & Caffrey (1998)	(18)
22:0/22:1c13 PC	32.8	Koynova & Caffrey (1998)	(18)

Table S4: Literature values of T_{melt} for PE-lipids

(Used for estimating T_{melt} values for vacuole lipids)

Chain length : unsaturation	T_{melt} (˚C)	Reference	Reference #
16:0/18:1 PE	24.41 ± 1.63 26.1	Koynova & Caffrey (1994) Wang *et al*. (1994)	(18)
18:0/18:1 PE	31.5 30.4	Wang *et al*. (1994) Silvius (1982)	(19, 21)
20:0/18:1 PE	33.9	Wang *et al*. (1994)	(21)
22:0/18:1 PE	34.3	Wang *et al*. (1994)	(21)
24:0/18:1 PE	35.2	Wang *et al*. (1994)	(21)
16:1/16:1 PE	-33.5	Koynova & Caffrey (1994) Silvius (1982)	(18) (19)
18.1/18.1 PE	-5.5 ± 0.5	Matsuki *et al*. (2017)	(23)

Table S5: How changes in lipid chain length and unsaturation affect T_{melt}
(Values are from Tables S2-S4)

Headgroup	Lipid 1, T_{melt}	Lipid 2, T_{melt}	Change in the average number of carbons (over both chains)	Change in the average saturation (over both chains)	Change in T_{melt} (per lipid)
PC	di(16:0)PC, 41.3˚C	di(17:0)PC, 48.6˚C	2	–	7.3˚C
PC	16:0/18:1PC, -1.6˚C	18:0/18:1PC, 6.7˚C	2	–	8.3˚C
PE	16:0/18:1PE, ~25˚C	18:0/18:1PE, ~31˚C	2	–	6˚C
AVERAGE EFFECT OF ADDING ONE CARBON PER LIPID					~ 7.2˚C
PC	18:1/18:1PC, -19.3˚C	18:0/18:1PC, 6.7˚C	–	1	26˚C
PC	18:1/18:1PC, -19.3˚C	18:1/18:0PC, 8.7˚C	–	1	28˚C
PE	18:1/18:1PE, -5.5	18:0/18:1PE, 31.0 ± 0.8˚C	–	1	37˚C
AVERAGE EFFECT OF ADDING ONE SATURATED BOND PER LIPID					~ 30.3˚C

Table S6: Differences in length of *sn*-1 and *sn*-2 chains of lipids from vacuoles in the log and stationary stages

Difference in number of carbons	Log stage (average ± standard deviation)	Stationary stage (average ± standard deviation
0 carbons	42.2 ± 1.1%	34.6 ± 2.6%
1 carbon	1.4 ± 0.3%	1.4 ± 0.9%
2 carbons	46.8 ± 0.7%	61.0 ± 2.1%
3 carbons	0.9 ± 0.5%	0.2 ± 0.1%
4 carbons	5.3 ± 0.3%	2.4 ± 0.1%
5 carbons	0.0 ± 0.0%	0.0 ± 0.0%
6 carbons	2.8 ± 0.1%	0.3 ± 0.2%
7 carbons	0.0 ± 0.0%	0.0 ± 0.0%
8 carbons	0.5 ± 0.2%	0.1 ± 0.1%
9 carbons	0.0 ± 0.0%	0.0 ± 0.0%
10 carbons	0.0 ± 0.0%	0.1 ± 0.1%

SUPPLEMENT REFERENCES

1. Reinhard, J., L. Starke, C. Klose, P. Haberkant, H. Hammarén, F. Stein, O. Klein, C. Berhorst, H. Stumpf, J.P. Sáenz, J. Hub, M. Schuldiner, and R. Ernst. 2022. A new technology for isolating organellar membranes provides fingerprints of lipid bilayer stress. *bioRxiv*. 2022.09.15.508072.

2. Brachmann, C.B., A. Davies, G.J. Cost, E. Caputo, J. Li, P. Hieter, and J.D. Boeke. 1998. Designer deletion strains derived from Saccharomyces cerevisiae S288C: a useful set of strains and plasmids for PCR-mediated gene disruption and other applications. *Yeast*. 14:115–132.

3. Huh, W.-K., J.V. Falvo, L.C. Gerke, A.S. Carroll, R.W. Howson, J.S. Weissman, and E.K. O'Shea. 2003. Global analysis of protein localization in budding yeast. *Nature*. 425:686–691.

4. Boothe, T., L. Hilbert, M. Heide, L. Berninger, W.B. Huttner, V. Zaburdaev, N.L. Vastenhouw, E.W. Myers, D.N. Drechsel, and J.C. Rink. 2017. A tunable refractive index matching medium for live imaging cells, tissues and model organisms. *Elife*. 6.

5. Ejsing, C.S., J.L. Sampaio, V. Surendranath, E. Duchoslav, K. Ekroos, R.W. Klemm, K. Simons, and A. Shevchenko. 2009. Global analysis of the yeast lipidome by quantitative shotgun mass spectrometry. *Proc. Natl. Acad. Sci. U. S. A.* 106:2136–2141.

6. Klose, C., M.A. Surma, M.J. Gerl, F. Meyenhofer, A. Shevchenko, and K. Simons. 2012. Flexibility of a Eukaryotic Lipidome – Insights from Yeast Lipidomics. *PLoS ONE*. 7:e35063.

7. Surma, M.A., R. Herzog, A. Vasilj, C. Klose, N. Christinat, D. Morin-Rivron, K. Simons, M. Masoodi, and J.L. Sampaio. 2015. An automated shotgun lipidomics platform for high throughput, comprehensive, and quantitative analysis of blood plasma intact lipids. *Eur. J. Lipid Sci. Technol.* 117:1540–1549.

8. Liebisch, G., M. Binder, R. Schifferer, T. Langmann, B. Schulz, and G. Schmitz. 2006. High throughput quantification of cholesterol and cholesteryl ester by electrospray ionization tandem mass spectrometry (ESI-MS/MS). *Biochim. Biophys. Acta*. 1761:121–128.

9. Herzog, R., K. Schuhmann, D. Schwudke, J.L. Sampaio, S.R. Bornstein, M. Schroeder, and A. Shevchenko. 2012. LipidXplorer: a software for consensual cross-platform lipidomics. *PLoS One*. 7:e29851.

10. Herzog, R., D. Schwudke, K. Schuhmann, J.L. Sampaio, S.R. Bornstein, M. Schroeder, and A. Shevchenko. 2011. A novel informatics concept for high-throughput shotgun lipidomics based on the molecular fragmentation query language. *Genome Biol.* 12:R8.

11. Ghaemmaghami, S., W.-K. Huh, K. Bower, R.W. Howson, A. Belle, N. Dephoure, E.K. O'Shea, and J.S. Weissman. 2003. Global analysis of protein expression in yeast. *Nature*. 425:737–741.

12. Ho, B., A. Baryshnikova, and G.W. Brown. 2018. Unification of Protein Abundance Datasets Yields a Quantitative Saccharomyces cerevisiae Proteome. *Cell Syst*. 6:192–205.e3.

13. Toulmay, A., and W.A. Prinz. 2013. Direct imaging reveals stable, micrometer-scale lipid domains that segregate proteins in live cells. *J. Cell Biol.* 202:35–44.

14. Zinser, E., C.D. Sperka-Gottlieb, E.V. Fasch, S.D. Kohlwein, F. Paltauf, and G. Daum. 1991. Phospholipid synthesis and lipid composition of subcellular membranes in the unicellular eukaryote Saccharomyces cerevisiae. *J. Bacteriol.* 173:2026–2034.

15. Benjamini, Y., A.M. Krieger, and D. Yekutieli. 2006. Adaptive linear step-up procedures that control the false discovery rate. *Biometrika*. 93:491–507.

16. Casanovas, A., R.R. Sprenger, K. Tarasov, D.E. Ruckerbauer, H.K. Hannibal-Bach, J. Zanghellini, O.N. Jensen, and C.S. Ejsing. 2015. Quantitative analysis of proteome and lipidome dynamics reveals functional regulation of global lipid metabolism. *Chem. Biol.* 22:412–425.

17. Tuller, G., T. Nemec, C. Hrastnik, and G. Daum. 1999. Lipid composition of subcellular membranes of an FY1679-derived haploid yeast wild-type strain grown on different carbon sources. *Yeast*. 15:1555–1564.

18. Koynova, R., and M. Caffrey. 1998. Phases and phase transitions of the phosphatidylcholines. *Biochim. Biophys. Acta*. 1376:91–145.

19. Silvius, J.R. 1982. Thermotropic phase transitions of pure lipids in model membranes and their modifications by membrane proteins. *Lipid-protein interactions*. 2:239–281.

20. Tada, K., E. Miyazaki, M. Goto, N. Tamai, H. Matsuki, and S. Kaneshina. 2009. Barotropic and thermotropic bilayer phase behavior of positional isomers of unsaturated mixed-chain phosphatidylcholines. *Biochim. Biophys. Acta*. 1788:1056–1063.

21. Wang, Z.Q., H.N. Lin, S. Li, and C.H. Huang. 1994. Calorimetric studies and molecular mechanics simulations of monounsaturated phosphatidylethanolamine bilayers. *J. Biol. Chem.* 269:23491–23499.

22. Koynova, R., and M. Caffrey. 1994. Phases and phase transitions of the hydrated phosphatidylethanolamines. *Chem. Phys. Lipids*. 69:1–34.

23. Matsuki, H., S. Endo, R. Sueyoshi, M. Goto, N. Tamai, and S. Kaneshina. 2017. Thermotropic and barotropic phase transitions on diacylphosphatidylethanolamine bilayer membranes. *Biochim. Biophys. Acta Biomembr.* 1859:1222–1232.

24. Goto, M., S. Ishida, N. Tamai, H. Matsuki, and S. Kaneshina. 2009. Chain asymmetry alters thermotropic and barotropic properties of phospholipid bilayer membranes. *Chem. Phys. Lipids*. 161:65–76.

25. Ichimori, H., T. Hata, H. Matsuki, and S. Kaneshina. 1999. Effect of unsaturated acyl chains on the thermotropic and barotropic phase transitions of phospholipid bilayer membranes. *Chem. Phys. Lipids*. 100:151–164.